ADVANCED MATERIALS
www.advmat.de

A Wearable All-Gel Multimodal Cutaneous Sensor Enabling Simultaneous Single-Site Monitoring of Cardiac-Related Biophysical Signals

*Kyoung-Yong Chun, Seunghwan Seo, and Chang-Soo Han**

The human cutaneous sensory organ is a highly evolved biosensor that is efficient, sensitive, selective, and adaptable. Recently, with the development of various materials and structures inspired by sensory organs, artificial cutaneous sensors have been widely studied. In this study, the acquisition of biophysical signals is demonstrated at one point on the body using a wearable all-gel-integrated multimodal sensor composed of four element sensors, inspired by the slow/rapid adapting functions of the skin sensory receptors. The gel-type sensors ensure flexibility, compactness, portability, adherence, and integrity. The wearable all-gel multimodal sensor is easily attached to the wrist and simultaneously gathers blood pressure (BP), electrocardiogram (ECG), electromyogram (EMG), and mechanomyogram (MMG) signals related to cardiac and muscle health. Human activity causes muscle contraction, which affects blood flow; therefore, the relationship between the muscle and heart is crucial for screening and predicting heart health. Cardiac health is monitored by obtaining the two types of phase time differences (i.e., Δt_{be}: BP and ECG, Δt_{em}: ECG and MMG) generated during muscle movement. The suggested multimodal sensor has potential applicability in monitoring biophysical conditions and diagnosing cardiac-related health problems.

1. Introduction

Human skin comprises excellent biological sensors with a complex mechanism that responds appropriately and cleverly to various external stimuli.[1] Recently, many tactile sensors inspired by the cutaneous sensory receptors of skin have been studied extensively, because natural sensors exhibit simultaneous multimodal sensations, high sensitivity, low energy consumption, flexibility, and small sizes, while performing multiple functions.[2] These advantages of the cutaneous sensory organ can have many applications, such as improving the sense of human motion, recognizing the surface of an object, and monitoring biosignals.[2a-c,3]

Recently, with the growing interest in health monitoring, many drawbacks pertaining to conventional sensor systems for acquiring biosignals have been identified; these include material limitations, complex manufacturing processes, portability difficulties, patient discomfort, and the hassle of multiple measurements. To overcome these shortcomings, wearable sensors that are easy to attach, portable, biocompatible, and multimeasurable are required. Wearable skin sensors can sequentially collect data without discomfort or interrupting daily activities, thereby enhancing user compliance with self-monitoring and improving the quality of patient care.[4] For example, several studies involving the monitoring of single physical parameters, such as electrocardiogram (ECG)[4d,e] and blood pressure (BP),[4f-h] using non-invasive wearable sensors have been reported. Given such remarkable findings, sensor integration has been shifting toward a combination of different sensor modalities.[5]

Recently, heart-health screening technology using the correlation of two or more biophysical signals has been attempted to prevent heart diseases and help maintain healthy human lives. In particular, the research on cardiac indicators involving the correlation between BP and ECG has attracted significant attention, with studies concerning the cardiovascular system being frequently reported.[6] In addition, heart health has also been predicted using the correlation between muscle contraction-related electromyogram (EMG)/mechanomyogram (MMG) and heart rate-related BP/ECG, which are biosignals related to muscle movements.[7] When muscle contractions occur under different environments, the fluctuations in the blood flow cause variations in the pulse, BP, and ECG; consequently, the measured data may be inaccurate, resulting in an inaccurate diagnosis. Therefore, diagnosing heart disease based on the strong correlation between biophysical signals can serve as a highly effective and reliable method. In addition, measuring these biophysical signals at a single part of the body using a multimodal sensor is desirable for ensuring stable and accurate readings.

Interestingly, BP and ECG exhibit slow adapting (SA) response characteristics, whereas EMG and MMG show rapid

K.-Y. Chun, C.-S. Han
Institute of Advanced Machinery Design Technology
Korea University
Anam-Dong, Seongbuk-Gu, Seoul 136-713, Republic of Korea
E-mail: cshan@korea.ac.kr
S. Seo, C.-S. Han
School of Mechanical Engineering
College of Engineering
Korea University
Anam-Dong, Seongbuk-Gu, Seoul 136-713, Republic of Korea
The ORCID identification number(s) for the author(s) of this article can be found under https://doi.org/10.1002/adma.202110082.

DOI: 10.1002/adma.202110082

adapting (RA)-like characteristic signals. Generally, in skin sensory receptors, the SA receptors respond to static touch and pressure, and the RA receptors respond to dynamic touch and vibration stimuli. Based on physiological studies, researchers have adopted various methods to mimic these properties of actual skin.[2,8] When the adaptive signals of SA and RA receptors, which play a critical role in detecting the shape, texture, and movement of an object, are implemented, an adaptive sensor can respond to the changes in the surrounding conditions in a smarter manner by acquiring a selective and broadband signal, as compared with the monotonous signal acquisition of conventional sensors.[9] However, existing artificial sensors require complicated manufacturing processes for the fabrication of individual components and complex combinations to build multimodal sensations. It is also difficult to obtain signals at the same time and location by distinguishing between the frequency band and pressure range, as in the case of the skin sensory organ.

To the best of our knowledge, wearable multimodal sensors that simultaneously measure multiple types of biophysical signals at the same location using SA and RA responses have not been studied thus far. In this work, we developed an artificial, wearable, all-gel multimodal cutaneous sensor with flexibility, ease of assembly, and integrity; this sensor can monitor four biophysical signals, namely, BP, ECG, EMG, and MMG, simultaneously at the wrist. The PANi–poly(vinyl chloride) (PVC) ionic composite gel was selected as a strategic material for SA properties such as BP and ECG, whereas the polyvinylidene fluoride-trifluoroethylene (PVDF-TrFe) gel was selected for the RA response properties and used to detect MMG. In addition, the PANi–PVC ionic gel was adopted as a conductive electrode suitable for measuring ECG signals. We evaluated cardiovascular health by simultaneously monitoring the correlation between muscle dynamics and hemodynamics, with respect to exercise and muscle movements. The proposed all-gel multimodal sensor can realize the comprehensive tracking of heart conditions in users' daily activities and also enable the collection of important data that can be used to predict heart conditions based on physical responses and exercise.

2. Results and Discussion

Numerous factors affect human cardiac health in relation to various activities and behaviors. The heart responds to external and internal information collected from various sensory organs. Among these sensory organs, the cutaneous organ plays a vital role in terms of survival and particularly detects various mechanical stimuli such as external pressures, strains, and vibrations. The artificial skin sensor developed using the characteristics of biological skin sensory receptors responds to changes in the electrical/mechanical stimulation inside and outside the skin, such as changes in the blood flow inside human skin and the current flowing through the skin or internal tissues (**Figure 1**a). In this study, a sensor module that can be easily attached to human skin and features an adjustable size, arrangement, and attachment position (Figure 1b) was developed. Four biophysical signals were simultaneously measured, with the ECG and EMG corresponding to electrophysiological signals and the BP and MMG signals corresponding to kinematic signals

The sensor comprises three flexible ECG electrodes composed of PANi–PVC gel with a sheet resistance of ≈10 kΩ $\square^{-1}$. Two electrodes, including the ground electrode, were in contact with the skin, and the other electrode was placed on the outer surface to be in contact with the other hand during measurement. The EMG sensor consists of three electrodes, which are PANi–PVC gels that are in contact with the skin surface. These two sensors employed the conductive gels as electrodes and obtained signals through an Arduino interface, before monitoring the signals using an oscilloscope. The BP and MMG sensors are self-powered, system-integrated sensors. The MMG sensor directly obtains the signals using the PVDF-TrFe gel with an interdigitated-type carbon electrode. The PANi–PVC in the BP sensor was built with a conical shape at the surface in contact with the PVDF-TrFe gel, in order to improve surface reactivity. The voltage changes caused by the charge distribution in PANi–PVC were measured via the polling of PVDF-TrFe owing to the pressure in the radial artery. In this study, polyaniline (PANi) was added to increase the response magnitude by up to five times, as compared to that in our previous results.[2e]

When muscles are used, contraction and extension occur repeatedly, and biophysical signals such as EMG or MMG are consequently generated. This affects the ventricular systolic movement in the heart, which causes changes in the blood flow rate and pressure and differentiates cardiac-associated biological signals such as ECG and BP. Furthermore, this results in a change in the phase time (Δt) between the signals generated during muscle contraction and the cardiac-related biological signals, which can serve as an important indicator of cardiac disease (Figure 1c). Interestingly, SA and RA response signals, which are unique characteristics of skin sensory receptors, resemble biophysical signals (Figure 1d). The ECG and BP signals were highly similar to the signal signatures observed in SA receptors. The static response curve of SA receptors is effective in terms of expressing the ECG and BP signals, because it can represents signals that characterize all the processes occurring between on and off events. However, as EMG and MMG are signals with high frequencies, the immediate RA characteristic signals are suitable for these biological signals. Therefore, biophysical signals corresponding to the SA reactions were obtained from materials based on the PVC gel, whereas biological signals corresponding to the RA reactions were obtained based on PVDF-TrFe. For the EMG signals, the PANi–PVC gel was used because a conductive electrode, such as an ECG, was required.

The gel-based sensor module used in this study can be easily worn on the wrist by assembling it in a medical patch (Figure 1e-i). The section where the BP and MMG sensors are connected is designed to be more sensitive to stimulation in an interdigital manner, as shown in the inset of Figure 1e-ii. In addition, the interface at which the surfaces of the BP and MMG sensors were in contact forms a conical shape, resulting in a more sensitive response. This has been described in detail in our previous study.[2e] A conductive polymer (PANi) was blended to improve the response magnitude, as compared with that of the previously used PVC gel, and the operation mechanism is presented in Figure S1 in the Supporting Information. Briefly, the PVDF-TrFe gel sensor, which has

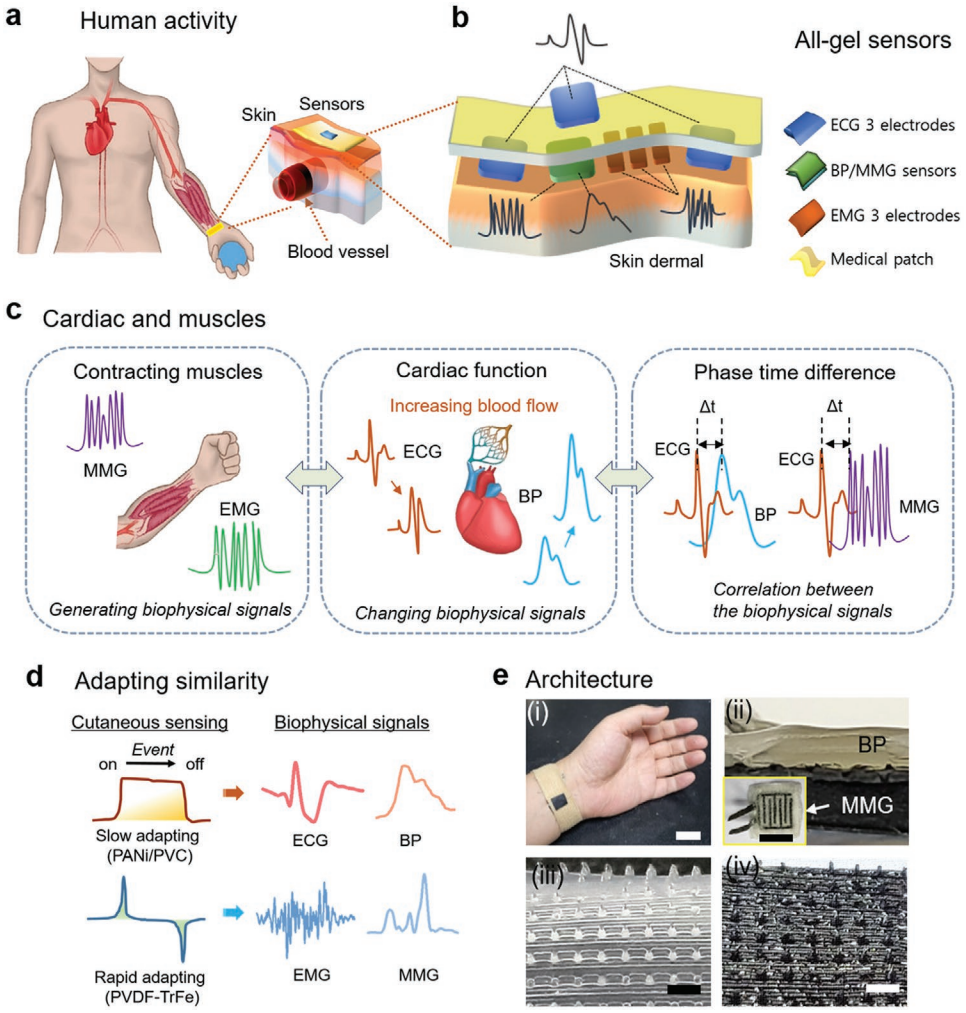

Figure 1. Schematics of artificial all-gel cutaneous sensor system and cardiac-related biophysical signals. a) Artificial gel sensor module attached to the skin close to a blood vessel, acquiring cardiac-related biophysical signals associated with human activity. b) Gel sensor module consisting of four component sensors: three electrodes for ECG, three electrodes for EMG, and combined BP sensor and ECG electrodes. c) Relationship between heart and muscle activity. EMG and MMG produced when using muscles. Variation in cardiac-related BP and ECG signals during muscle use. Correlation between PTD of biophysical signals. d) SA and RA signals generated from skin sensory receptors were similarly observed in the biophysical signals. SA receptor implementation using PANi–PVC gel and RA receptor implementation using PVDF-TrFe gel. e) Sensor architecture. i) Sensor module attached to the wrist (scale bar: 2 cm). ii) Stacked BP and MMG sensors (inset: interdigital-type MMG sensor, scale bar: 0.8 cm). iii) Surface morphology of PVDF-TrFe gel (scale bar: 0.5 mm). iv) Surface morphology of PANi–PVC gel (scale bar: 0.5 mm).

a built-in interdigital carbon electrode serving as the MMG sensor, obtains an electrical signal of muscle movement from the separated electrodes on both sides, as shown in the inset of Figure 1e-ii. At this time, the polarization in the PVDF-TrFe gel caused by pulse or muscle movement in the radial artery alters the charge distribution of the PANi–PVC gel, thus converting the change in the mechanical stimuli of the skin into an electrical signal. These material properties were derived from the unique structural bond of the polymers (Figure S2, Supporting Information). A certain degree of flexibility and stretchability can be ensured by adding dibutyl adipate (DBA), a plasticizer, to PVC and PVDF-TrFe. In addition to improving the electrical properties, as shown in Figure S3 in the Supporting Information, the molecular space of the phytic acid in the PANi sol can facilitate the function of capacitance and the movement of the cation and anion charges of the zwitterionic liquid (IL). These structural features play a positive role in exerting the SA characteristics. Because it is a THF-based PVC solution, the aqueous-based PANi sol was completely dried and then added to the PVC solution (Figure S4a, Supporting Information). Figure 1iii,iv shows the surface images of the PVDF-TrFe gel and PANi–PVC ion gel, respectively. To improve the sensitivity of the sensor, the surface was modified into a conical shape. The final process of manufacturing an individual sensor from the gel solution is illustrated in Figure S4b in the Supporting Information. Detailed information regarding the dimensions and the images of sensors are presented in Figure S5 in the Supporting Information.

Furthermore, through FT-IR analysis, it was confirmed that the blending was performed well in relation to the reaction (Figure S6, Supporting Information). Briefly, the characteristic peaks of the PVC gel, including the peaks for C—H bands, were

present at 1427 and 1257 cm^{-1}; the peaks for C—C vibrations were present at 968 cm^{-1}, whereas those for the C—Cl bands were noted at 698, 636, and 605 cm^{-1}. The peak at 1732 cm^{-1} corresponded to the carbonyl group (C=O) bands of DBA in the PVC gels.[10] In addition, the bands at 1295, 1241, and 1125 cm^{-1} were ascribed to the C—N and C—H bending of the benzenoid and quinoid rings of PANi.[11] When blending PANi with the PVC gel, characteristic peaks were observed, thereby confirming a successful synthesis.

The mechanical and electrical properties of the PVC and PVDF-TrFe gels have a considerable influence on the sensor's performance. In general, these two properties often appear opposite to each other, and thus, an appropriate trade-off is required. The sheet resistance and elongation of the PANi–PVC gel according to the amount of PANi in the PVC sol were obtained through an experiment; their correlation is shown in Figure S7 in the Supporting Information. From this figure, it is evident that the elongation and sheet resistance decrease as the amount of PANi increases. The lowest sheet resistance, accompanied by adequate elongation, was obtained at ≈15 vol% PANi. Accordingly, the amount of PANi was fixed at 15 vol% over the amount of PVC gel used for fabricating the sensor. Elongation was measured using an in-house strain machine, as shown in Figure S8 in the Supporting Information. Moreover, based on the various deformations, it is apparent that the sensor is highly flexible (Figure S5b, Supporting Information). At 15 vol% PANi, an elongation of ≈200% was obtained. When the amount of PANi exceeded 15 vol%, the PANi–PVC gel was easily broken, even under slight tension.

The results of cyclic voltammetry (CV) differed considerably depending on the content of the IL contained in the PANi–PVC gel. As the IL content increased, significantly larger currents flowed under the same voltage conditions, and the capacitance function was improved (**Figure 2**a). Thus, an appropriate amount of IL is required, because, when an excessive amount of IL was used, it leaked out. In this study, 0.2 wt% IL versus PVC sol was used, which is almost consistent with that employed in a previous study.[5d] The addition of PANi has a week influence on the impedance characteristic of the PVC gel (Figure 2b). This is attributed to the structural characteristics of PANi, including its molecular spatiality, as shown in Figure S3 in the Supporting Information. Figure 2c shows the voltage characteristics measured when a constant pressure (150 Pa) is applied to the PANi–PVC gel, while gradually increasing the voltage. The inset of Figure 2c presents the output voltage curves measured under the application of various pressures for ≈2 s. Based on these observations, it was concluded that the curves follow the SA characteristic response. From this basic result, the maximum value of each output voltage was obtained, and the linear proportional value was determined, as shown in Figure 2c. In this study, because PVDF-TrFe (which generates a voltage under 10 mV at the same pressure) was used as the voltage source, the measurement test voltage was set to less than 10 mV. The output voltage curve of the PVDF-TrFe gel obtained while changing the pressure for 1.3 s, presented in Figure 2d, shows that the voltage increases with the variations in pressure. The inset in Figure 2d depicts the output voltage curves of the PVDF-TrFe gel under various pressures. Based on these plots, a typical piezoelectric characteristic was noted, which is suitable for indicating RA responses.

In addition to the individual pressure response characteristics of the PANi–PVC gel and the PVDF-TrFe gel, when these two gels are superimposed, two SA and RA response characteristics can be obtained with one sensor module. Figure 2e shows the voltage changes caused by pressure variations, as obtained from the two integrated gel sensors. The structure of the integrated gel sensor is illustrated in Figure S1 in the Supporting Information. The contact surfaces of the PANi–PVA and PVDF-TrFe gels were configured with a conical structure to improve sensitivity. This operating mechanism is similar to that reported in a previous study,[2e] except for the capacitive function of PANi, which makes it effective in terms of measuring responses. Actual SA response signals, such as the BP, were acquired from the PANi–PVC gel region. As can be seen from the inset of Figure 2e, an SA characteristic curve was obtained, and the sensitivity curve was formed with a tendency to converge above ≈120 Pa. The pressure sensitivity in the region up to ≈120 Pa was $\approx 9.7 \times 10^{-1}$ V kPa^{-1}. When a pressure of ≈120 Pa was applied to the sensor, the initial and terminal response times were both approximately 200 ms. The inset of the Figure 2e indicates the conditions of the applied pressure. As shown in Figure 2f, owing to the nature of the gel, a response delay exists in the elastic region when a pressure is applied; however, the actual response rate is highly similar to the initial and terminal times of the input pressure curve. As shown in Figure 2g, the output voltage was measured while applying a pressure of ≈160 Pa on the PANi–PVC/PVDF-TrFe gel-integrated sensor approximately one month after manufacture. It was thus confirmed that electric signals with respect to pressure could be obtained in a stable manner. As these gels are not hydrogel-based, it is possible to maintain their performance for a long period, unlike hydrogel-based sensors.

In general, bioelectrodes can be categorized into two types: dry and wet bioelectrodes. Conventional dry electrodes (metal or polymer) feature poor adhesion to skin and a high modulus; they are also mechanically inconsistent with soft skin, which can degrade the signal quality.[12] Thus, research is being devoted toward improving the flexibility and adhesion of dry electrodes. Moreover, a typical hydrogel in wet electrodes can be realized by combining conductors with high conductivity, owing to its own high resistance.[13] Therefore, current research is mainly focused on bioelectrodes for the purpose of achieving a high signal-to-noise ratio (SNR) and improving the body adhesion suitability. Notably, the PANi–PVC ion gel has a resistance of ≈600 kΩ, a conductivity of ≈890 mS/cm, and a SNR of ≈120, which are higher or comparable to those of conventional hydrogel-based bioelectrodes.[14] Accordingly, the PANi–PVC ion gel can be suitable for use as a bioelectrode. However, longer-term experiments will be needed to determine whether the use of this gel can lead to skin allergies, as in the case of conductive hydrogels in contact with skin[2d]

$$C = \left(\frac{1}{R}\right) \times \left(\frac{l}{A}\right) \tag{1}$$

where C is conductivity of the ion gel, R is the gel resistance, l is the thickness of the gel, and A is the area of the electrode surface in contact with the gel

$$\mathrm{SNR} = \frac{P_{\mathrm{signal}}}{P_{\mathrm{noise}}} = \left(\frac{A_{\mathrm{signal}}}{A_{\mathrm{noise}}}\right)^2 \tag{2}$$

where, A_x is the root mean square of the signals.

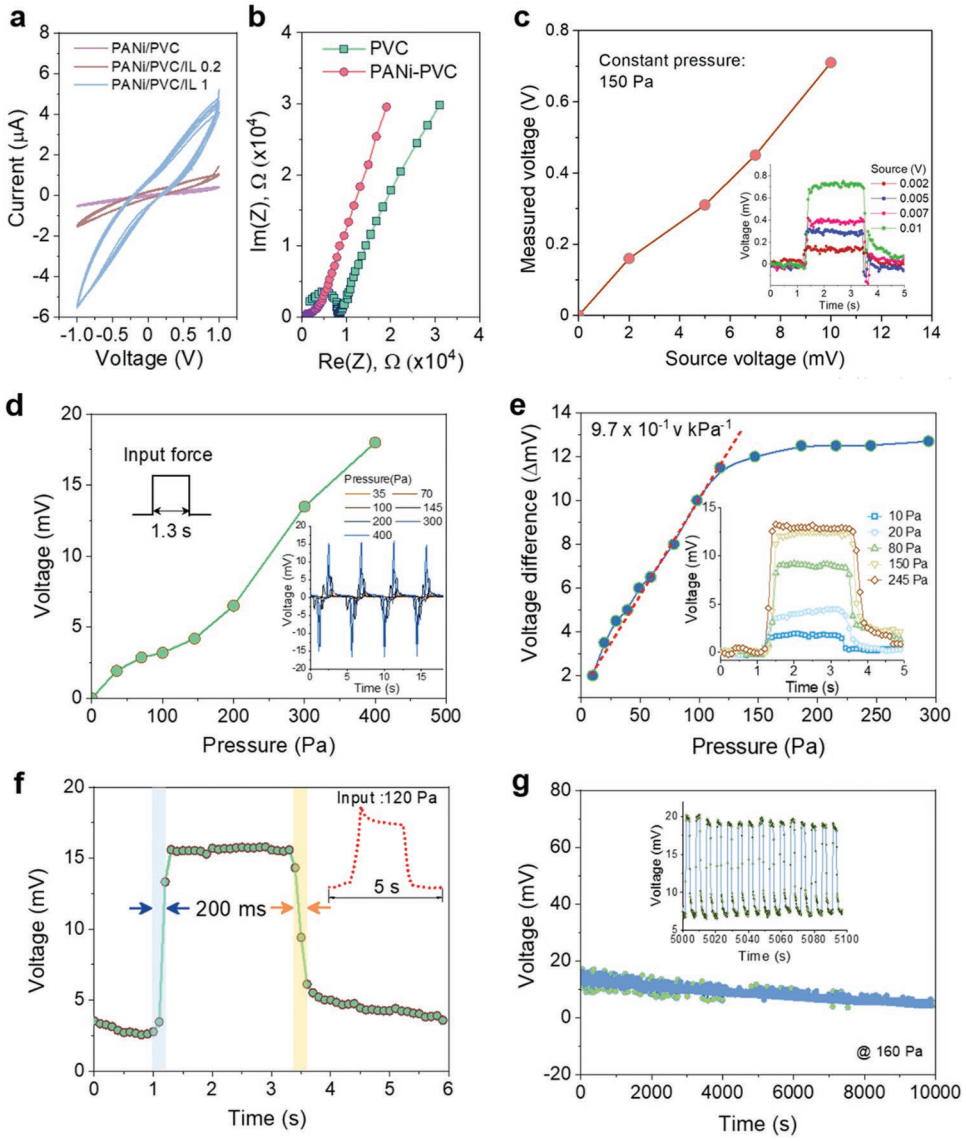

Figure 2. Characterization of artificial gel cutaneous sensors. a) PANi–PVC gel CV characteristics according to amount of IL. b) Impedance characteristics of PVC and PANi–PVC. c) Relationship with measured voltage according to changes in source voltage of the PANi–PVC gel under ≈150 Pa. (Inset: output voltage of SA characteristic) d) Voltage generation plot for PVDF-TrFe gel according to pressure changes (Input force during 1.3 s). (Inset: voltage generation curve with time; similar to RA characteristic). e) Characteristic curve of PANi–PVC/PVDF-TrFe self-powered integrated sensor. A linear increase in generated voltage was observed up to ≈120 Pa, depending on the pressure. Sensitivity: 9.7×10^{-1} V KPa^{-1}. (Inset: SA-like sensor characteristic according to pressure change). f) Initial and terminal response times of ≈200 ms. (Inset: ≈ 120 Pa input force curve for 5 s). g) Examination of sensor stability under 160 Pa. (Inset: expanded output signal in a certain time section).

Four biophysical signals were measured under various conditions to evaluate the performance of the individual sensors. The tests involved a healthy male volunteer in his mid-50s who had no history of heart disease. First, kinematic signals corresponding to the BP and MMG were separated into two channels in the stacked sensor; using an oscilloscope, the BP was obtained from the Ag electrode connected to the PANi–PVC gel (**Figure 3**a). The pulse rate and BP curves were identified based on the changes in the voltage measured under rest and post exercise conditions (Figure 3b). For more intuitive monitoring, BP was estimated by matching between the output voltage from a PANi–PVC gel sensor and actual simultaneous measurement with a commercial BP monitoring instrument (Omron, HEM 6311). For the systolic blood pressure (SBP), $y = 2.6x + 93.5$ ($R = 0.91$) was derived; for the diastolic blood pressure (DBP), $y = 3.1x + 63.1$ ($R = 0.9$) was determined. Based on these equations (inset of Figure 3c), the changes in voltage were converted into BP levels and subsequently plotted. P1 and P2, which denote the characteristic peaks between the systolic and diastolic BP, were also confirmed (Figure 3c). The trend of the changes in the raw BP curve over a longer period of time can be observed in Figure S9 in the Supporting Information. When the gripper was used, the change in BP tended to increase with the grip strength (Figure 3d). These results represent an

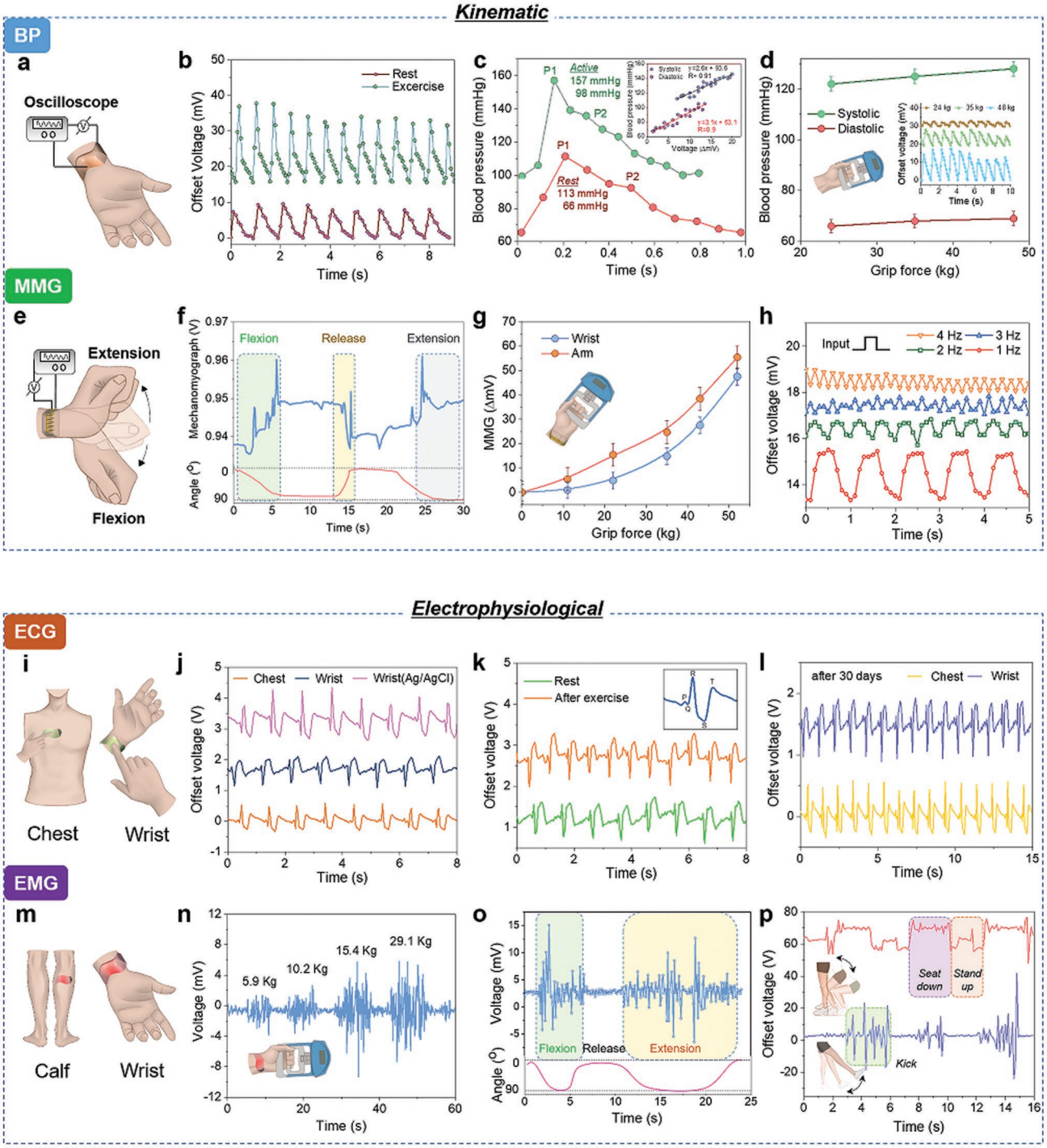

Figure 3. Characterization of kinematic (BP and MMG) and electrophysiological (ECG and EMG) component sensors. a) Wrist-mounted BP sensor measurement with oscilloscope. b) BP signal at rest and after exercise (fast walking). c) Conversion of BP voltage signal to BP value (mmHg) in the resting state and after exercising (fast walking). (Inset: Derivation of systolic and diastolic BP relation from BP curve according to voltage change). Systolic: $y = 2.6x + 93.9$ ($R = 0.91$), and diastolic: $y = 3.1x + 63.1$ ($R = 0.9$). d) Systolic and diastolic changes under grip force. (Inset: generated voltage curve according to grip force). e) MMG sensor attached to wrist and expressions for flexion and extension. f) MMG signal according to wrist angle. g) Signal values from MMG sensor attached to the arm and wrist according to grip force. h) Voltage generation of MMG sensor according to frequency changes. i) ECG sensors attached to chest and wrist. j) Signal obtained by ECG sensor. Comparison with commercial ECG (Ag/AgCl). k) Comparison of ECG signals at rest and after exercise (light walking). (Inset: typical ECG signal and main peaks) l) ECG measurements for sensor stability after 30 days. m) EMG sensors attached to calf and wrist. n) EMG signal measured while increasing gripper force. o) EMG signal measured while changing wrist angle. p) Signal acquisition according to activity type of EMG sensor attached to calf. (Top: standing and sitting down, bottom: kicking).

attempt at indirectly indicating the correlation between muscle contraction and cardiac pulsation and can serve as the basis for determining the association between MMG and EMG.

MMG, one of the signals generated during muscle contraction, was obtained from the PVDF-TrFe gel, with the interdigital carbon electrodes attached to the wrist for several muscle movements (Figure 3e). A large voltage change was observed depending on the movement of the wrist, and fluctuations in the signal were also confirmed according to the degree of muscle contraction, even during movement. Based on these signals, the trend of the signals distinguished from muscle contraction and relaxation was determined; it was confirmed that signal deviations occurred even in the case of variations in the gripping force. In addition, MMG signals were acquired and plotted based on isometric muscle contraction using a grip force (Figure 3g). The MMG signals obtained from the sensors attached to the wrists and arms were similar; however, the values obtained from the arm were slightly larger. In addition, as the input frequency increased, the MMG response cycle increased but the voltage amplitude decreased (Figure 3h). Thus, the fabricated MMG sensor exhibits frequency responsiveness.

Unlike the above kinematic signals, three or more conductive electrodes are generally required to measure electrical and physical biological signals. In hospitals or clinics, for ECG measurements, ≈12 electrodes are attached to the chest, arms, and legs to obtain complementary information regarding the heart. However, a portable, simple, three-electrode ECG device was recently developed and commercialized. In this study, the ECG and EMG signals based on three gel electrodes were measured as components of the integrated sensor. Figure 3i shows the measurement method for the ECG sensor attached to the chest and wrist. The positive and ground electrodes were brought into contact with the skin surface, and the measurement was performed by touching a finger of the other hand to the negative electrode exposed on the outside of the patch. Figure 3j compares the ECG signals obtained from the chest and wrist under a stable state; these results were measured using a commercial Ag/AgCl ECG electrode. It was confirmed that the typical P, Q, R, S, and T peaks appeared in the ECG signal, and the T peak increased when measured at the wrist (inset of Figure 3k). The ECG signals measured at the wrist during rest and after light exercise were compared (Figure 3k). The change in the pulse rate was determined based on the ECG peaks (rest: ≈60, and after exercise: ≈83); moreover, the T value after exercise was relatively elevated. A typical ECG electrode uses a metal or hydrogel-based electrode. However, in the case of a metal electrode, discomfort is caused when it comes in contact with the skin surface, and the creation of a conformal state on the skin surface is also difficult. Hydrogels also tend to dry easily during continuous use under general conditions, thereby making it difficult to ensure accurate measured values after a certain period of time. In this study, as a non-hydrogel-based gel electrode was employed, stability was maintained, even during measurements after approximately a month after initial measurement (Figure 3l).

In the case of EMG, the signals were obtained through three gel electrodes in contact with the skin on the wrist and calf (Figure 3m). The magnitude of the signals increased with the force applied by the gripper (Figure 3n). Despite the disadvantage that EMG signals interfere with the electric field or current flow inside and outside the body, EMG could play a complementary role, as compared to the MMG signal. In addition to the muscle contractions due to mechanical force, the EMG signals were also measured during the flexion and extension of the wrist. Unlike MMG signals, these signals exhibit a shape more similar to the RA characteristics (Figure 3o). Figure 3p presents the signals for isotonic muscle movement during standing and sitting and the signals during kicking, as obtained through the ECG sensor attached to the calf. Distinctive EMG signals were obtained for two different behaviors, indicating that various human movements could potentially be categorized.

Figure 4 presents information regarding the heart, obtained by simultaneously acquiring four biophysical signals from the integrated gel sensor module. As shown in Figure 4a, each sensor in contact with the skin is indicated at the top, and one electrode of the ECG is placed outside the medical patch. A simple method was used for attaching the sensor to a medical patch, and the position of each sensor was based on placing the BP/MMG sensor at the radial artery site (i.e., where the pulse was measured). Figure 4b shows the circuit diagram for the signal acquisition of an integrated sensor. PANi–PVC performs the sensory functions for BP, ECG, and EMG, consisting of the capacitance, resistance, and Warburg impedance; PVDF-TrFe measures MMG indicating as resistance and voltage generation. Signal conversion was performed using the Arduino interface (AD8232: ECG, AD8226: EMG). A detailed description is provided in Figure S10 in the Supporting Information. The MMG and BP sensors were set in a stacked configuration. As shown in Figure 4c, the integrated sensor thus configured could obtain electrophysiological and kinematic signals from each component sensor simultaneously and then monitor them through an oscilloscope with four channels (Figure 4c). The correlation determined through the acquisition of four signals can be useful for screening cardiac health. In other words, predicting heart disease using the relationship between the phase difference (Δt_{be}) of BP and ECG, known as the pulse transit time (PTT),[6b,c,7] and the phase difference (Δt_{me}) of MMG and ECG, has recently been introduced by some researchers.[15] It has been reported that the phase time difference (PTD) between cardiac and muscle contractions strongly influences the BP and cardiac afterload during intermittent muscle contraction. Thus, the clinical application of a well-designed stimulator that induces a combination of heart rate and muscle contraction by maintaining an appropriate phase difference can support the concept of inducing a low SBP and cardiac afterload. Kirby et al. reported that heart rhythms are associated with cycling of a certain muscle intensity; however, the essential beat-by-beat analysis for understand this coupling phenomenon has been lacking.[16] Kimura et al. also demonstrated the afterload through the PTD in muscle contractions electrically synchronized with the heart rate during intermittent electrical stimulation.[17] However, physiologically, many areas of analysis and algorithm still need to be developed, and further research is warranted.

The four biophysical signals measured during the rest period are shown in Figure 4d. During this period, the EMG and MMG signals were negligible, whereas the ECG and BP signals

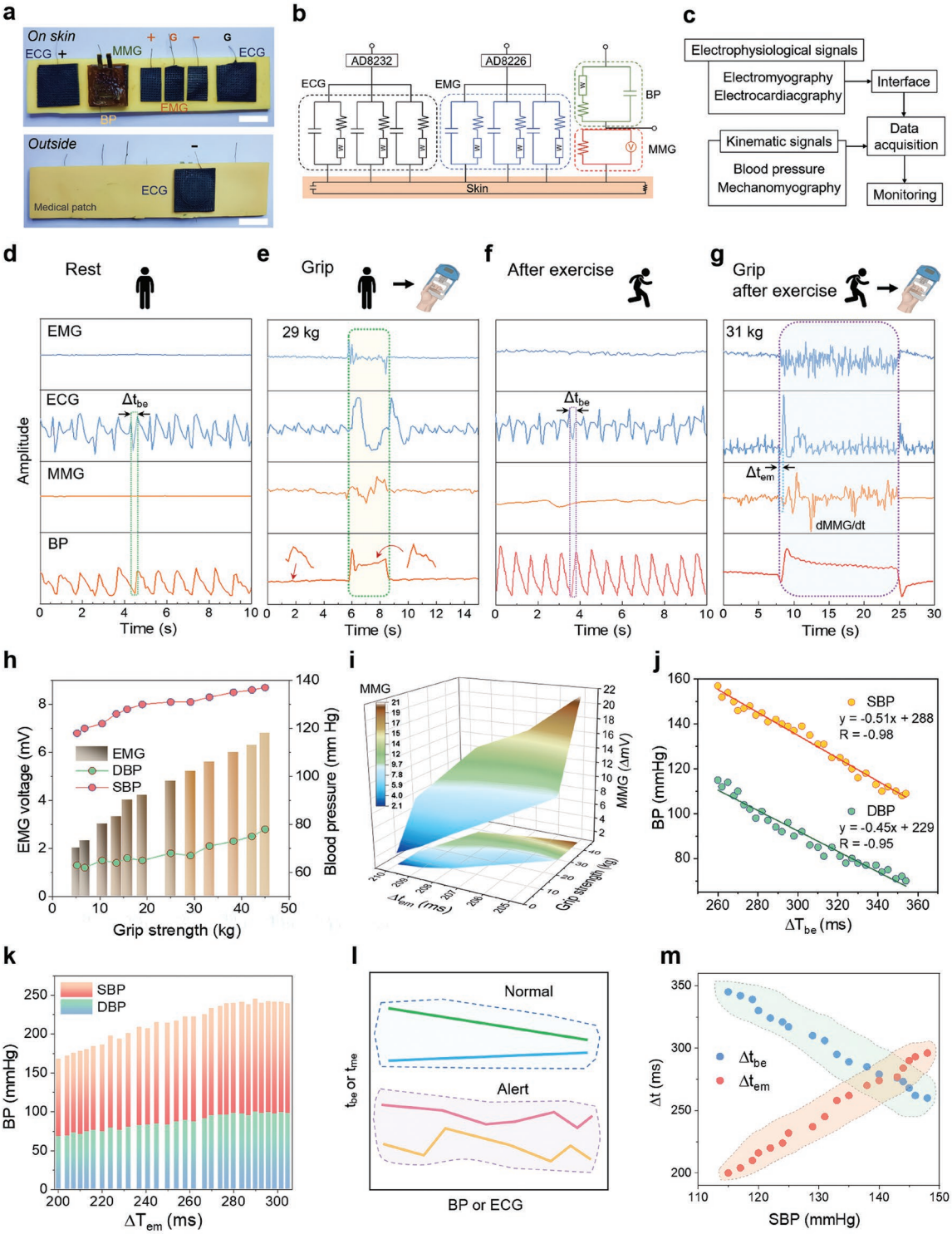

Figure 4. Simultaneous measurement and characterization of biophysical signals from integrated gel sensors. a) Photograph of integrated sensor module with four component sensors (scale bar: 1 cm). (Top: sensors on skin, bottom: ECG electrode on the outside the medical patch). b) Each sensor circuit consists of resistance, capacitance, and Warburg impedance. c) Simple flowchart for measuring and monitoring biophysical signals. d) Measuring biophysical signals at rest and defining Δt_{be}. e) Biophysical signals measured during gripping (29 kg). f) Postexercise (light running) biophysical signals and Δt_{be}. g) Biophysical signals measured while gripping after exercise (light running). MMG is a differential signal. Definition of Δt_{em}. h) Changes in EMG and BP (SBP and DBP) according to grip strength. i) Relationship between MMG and Δt_{em} with respect to grip strength. j) Derivation of relationship between BP (SBP and DBP) and Δt_{be} (SBP: $y = -0.51x + 288$, $R = -0.98$; DBP: $y = -0.45x + 229$, $R = -0.95$). k) Change in BP values according to Δt_{em}. l) Prediction chart between BP value and PTD (healthy state and risky state). m) Correlation between Δt_{be} and Δt_{em} with respect to variations in SBP.

were clearly obtained, as usual. In this case, the PTD between the R peak of the ECG and the P1 peak of BP, known as the PTT, is referred to as Δt_{be}. In addition, the four biophysical signals appearing during isometric muscle contraction at rest are shown in Figure 4e. When a grip force of 29 kg was applied, the output voltages of the EMG and MMG were obtained in the form of the signals of RA receptors. In addition, the BP and ECG signals also exhibited signal deformation due to muscle movement. Nevertheless, it was difficult to obtain intact ECG signals. Although the voltage baseline was moved, the BP curve could be obtained immediately. Thus, it can be concluded that the tendency of each biophysical signal to vary with respect to muscle contractions is unique. Furthermore, the EMG and MMG signals obtained after light running were slightly different from those at rest. However, there was no direct movement of the muscle; therefore, a change in the cognitive signal was not confirmed (Figure 4f). During the gripping after exercise, four distinct signals were obtained, as shown in Figure 4g. Compared to that in Figure 4e, gripping was continued for a longer time (≈15 s), and clear ECG and BP signals were acquired. The phase difference (Δt_{me}) between the R peak of the ECG and the initial firing peak of the MMG was obtained using the differential value, in order to acquire the MMG signal more clearly. At this time, the EMG is an important signal that mutually confirms the firing peak of the MMG. In general, the EMG is a biophysical signal used for muscle movements; however, the MMG is preferred owing to the electromagnetic interference inside and outside the body when obtaining electrical signals such as the ECG.[18] In this study, it was confirmed that the phase difference between the EMG and MMG was small. To assess the repeatability of the four biophysical signals, the signal change according to the grip (≈31 kg ± 3) after exercise was evaluated, as shown in Figure S11 in the Supporting Information. A similar trend could be confirmed under constant grip strength conditions.

Various analyses can be performed using the four biophysical signals obtained simultaneously. As shown in Figure 4h, the change in the EMG signals according to the distribution of BP during gripping was tracked. As the grip strength increased, the level of EMG increased almost linearly; however, there was no significant change in either the SBP or the DBP. This was attributed to the isometric muscle contraction; the use of larger muscles and a longer duration of gripping would result in a different magnitude. In addition, it was shown that the MMG signal magnitude increases with the grip strength in the resting state; however, the variation in Δt_{em} was significantly small (between 205 and 210), such that it did not have a notable effect on the phase difference (Δt_{em}) (Figure 4i). Conversely, this result implies that the irregularities in heart-related biophysicals (Δt_{em} irregularities or large phase difference) when using weak muscles in the resting state may indicate a red alert for heart health. Before and after exercise, the distribution of the BP according to the increase in Δt_{be} and Δt_{me} can be checked during muscle movement through gripping. Δt_{be} exhibited a tendency to decrease with an increase in the SBP and DBP. For the SBP, which is directly related to the left ventricle in heart disease, $\gamma = -0.51 \times 268$ ($R = -0.98$) was determined (Figure 4j). Under the same conditions, Δt_{me} showed a tendency to saturate at ≈280 ms (Figure 4k).

In a healthy heart, Δt_{be} or Δt_{me} shows a correlation in a certain BP or ECG region; however, in the case of a cardiac disease such as arrhythmia, irregular phase time changes would appear (Figure 4l).[15b,16] This screening method offers the advantage of obtaining additional information, and it can be more reliable than determining heart-health indicators using conventional PTT methods such as the BP and ECG. According to the change in the SBP, as shown in the Figure 4m, the relationship between Δt_{be} and Δt_{me} tends to be inversely proportional. Thus far, it has been difficult to physiologically derive a clear link between these two PTDs; however, many relevant studies are currently underway. It is also expected that a linear relationship exists between the BP and phase time, at least under healthy heart conditions. This result, considering the previous studies that predicted heart disease based on an irregular PTD or the maintenance of the PTD within a safe range using electrical stimulation therapy, is highly encouraging for cardiac disease care.

Although, one of the effective areas for the immediate application of gel-based sensors is the field of medical devices, appropriate guidelines or health indicators associated with the correlation between heart-related biosignals and muscle movement-related biosignals are still limited. Nevertheless, certain researchers have devoted efforts toward studying these correlations in order to develop suitable algorithms for wearable sensor devices.[15b,16,17,19] With regard to the heart health diagnosis approach proposed herein, to obtain data pertaining to Δt_{be} and Δt_{em} and establish an accurate algorithm based on these data, it is necessary to incorporate the acquired data with artificial intelligence-based techniques. In particular, it is essential to expand the number of subjects according to various conditions, such as age, gender, and environment, and conduct a sample survey involving normal and diseased people.

3. Conlusion

A wearable compact gel sensor inspired by human cutaneous sensory receptors was developed in this study. Using this sensor, human biophysical signals were simultaneously measured, and their correlations were investigated. For this purpose, the PANi–PVC composite gel and PVDF-TrFe gel, which can recognize the signal characteristics of SA and RA receptors (characteristics of biophysical sensors), were used. The fabricated sensor is a customized, portable integrated sensor that enables convenient manufacturing and architectural design. Thus, four biophysical signals—BP, ECG, EMG, and MMG—were successfully acquired simultaneously, and the correlation between cardiac and muscle movements was discussed. Cardiovascular-related biophysical signals vary according to muscle contractions; hence, a method for predicting or screening cardiovascular diseases based on the PTD between muscle contraction-related biophysical signals (MMG and ECG) and cardiovascular-related biophysical signals (BP and ECG) generated during muscle contraction is considerably important. In addition, using this type of sensor and the analysis method, representative diseases that cause symptoms such as heart failure due to excessive afterload (including hypertension, aortic stenosis, and pulmonary valve stenosis) could be screened or

even prevented. Regarding the novelty of this work, a sensitive pressure sensor was manufactured, while maintaining the flexibility and elasticity of the conventional PVC ion gel. Owing to their conductivities, PVC–PANi-based ion gel sensors can measure pressure-related biophysical signals as well as electrophysiological signals. It is also worthwhile to fabricate a flexible pressure sensor capable of measuring biosignals by manufacturing PVDF-TrFe in a gel-type form. These are considerably valuable results, and the proposed sensor can be also applied in many different fields as a multimodal sensor.

4. Experimental Section

Materials: PVC was purchased from Scientific Polymer Products Inc., and commercial PVDF-TrFe powder was purchased from Piezotech (FC30). DBA was obtained from TCI Chemicals, and (1-ethyl-3-methylimidazolium bis (trifluoromethylsulfonyl) imide) to be used as the IL and tetrahydrofuran were purchased from Sigma-Aldrich. Aniline, ammonium persulfate, and phytic acid were purchased from Sigma-Aldrich. All the chemicals were used without purification or pretreatment. PVC gel was prepared by fixing the weight ratio of PVC/DBA/IL to 1:2:0.2. For the PVDF-TrFe gel, the ratio of PVDF-TrFe/DBA was 1:2. PANi was prepared based on a previously reported method.[2f] Briefly, 0.286 g (1.25 mmol) of ammonium persulfate was dissolved in 1 mL of deionized water. An aniline solution was prepared by mixing 0.921 mL (1 mmol) of phytic acid, 0.458 mL (5 mmol) of aniline, and 2 mL of DI water. After the PANi was sufficiently dried in a drying oven, it was blended with PVC gel under a certain volume ratio.

Fabrication of Gel Sensors: A conical structure was formed via drop casting on a mold (1.5×1.5 cm^2, depth: 0.5 mm) through the surface modification of the PANi–PVC gel and PVDF-TrFe gel. To obtain a signal from the gel sensor, Ag wires and interdigital-type carbon electrodes were inserted into the PVC and PVDF-TrFe gels, respectively. The PVDF-TrFe surface in contact with PANi–PVC was coated with carbon graphite in the stacked sensor structure used for the BP and MMG measurements. The sensors composed of the PANi–PVC gel were used to measure the BP, ECG, and EMG. In particular, for the ECG and EMG sensors, which were composed of the conductive electrodes, PANi:PVC was fixed uniformly at a volume ratio of 0.15:1. The PVDF-TrFe gel was used to extract the MMG signal, and an interdigital-type carbon electrode (8×8 mm^2, line width: 0.6 mm) was installed as the internal electrode. All the sensors were fabricated with a conical structure to maintain a conformal state, wherein they are in contact with the skin and the side attached to the medical patch remains flat. In addition, all the electrodes and sensors were in contact with the skin, except for the ECG electrode located outside the medical patch.

Characterization of Materials and Sensors: FT-IR (PerkinElmer, Frontier) was used in the range of 400–4000 cm^{-1} to confirm the degree of synthesis of the PANi–PVC gel. CV was conducted and the impedance of the PANi–PVC gel was measured using a potentiometer (Princeton Applied Research, VersaSTAT 3) under an applied voltage supplying voltage. To apply an external force to the PANi–PVC and PVDF-TrFe gel sensors, a home-built computer system consisting of a stepping motor and a force tip was utilized with varying frequencies. Simultaneously, the output voltage from the sensor was measured by connecting to a four-channel oscilloscope (Tektronix, MDO 4024C).

Measurement of Four Biophysical Signals Using Component Sensors: The BP and MMG sensors featured a stacked structure. First, the MMG sensor in contact with the skin receives a signal from the two carbon electrodes. The BP sensor located at the top emits a signal through the Ag wire installed in the PANi–PVC and is monitored by an oscilloscope. The stacked BP and MMG sensors were installed such that they were in contact with the location of the radial artery. Here, both the BP and MMG sensors are self-powered sensors. The EMG sensor is composed of three PANi-PVC gels with an area of 1.5×0.8 cm^2 arranged side by side, and signals were extracted from each electrode through the Ag wire. The ECG sensor is composed of two PANi-PVC gel electrodes with an area of 1.7×1.7 cm^2 placed in contact with the skin. One electrode is attached to the outside of the medical patch, and this exposed electrode is touched using the finger of the opposite hand for measurements. The BP and MMG signals were measured during sitting without any body movement, following the wrist angle change, rest, and exercise. In addition, the state of the body was maintained in a stable manner during the measurements, even after the isometric muscle contraction through gripping. When measuring the MMG, the output voltage was measured under a state where a constant force was applied within the limited frequency range of the force sensor. For the ECG, two electrodes arranged side by side were directly attached to the chest or wrist, while the other electrode located outside the patch was operated as a three-electrode cell by connecting with the finger of the other hand. The measured signals were compared with those from a commercial ECG electrode equipped with a conventional hydrogel-based Ag/AgCl electrode. The EMG sensor was mounted on the wrist to measure the changes in the signal with respect to the variations in the gripping and wrist angle. The EMG sensor was also mounted on the calf to obtain the changes in the signal during standing, sitting, and kicking. These ECG and EMG signals were obtained through an Arduino module (AD8232, AD8226) with a power source of 3 V. These tests involved a male participant in his mid-50s, who went through repeated experiments under the same conditions for four weeks.

Characterization of the Integrated Artificial Gel Cutaneous Sensor: The four-element sensors were sorted in a uniform arrangement on a medical patch. After mounting the BP/MMG sensor at the radial artery position, the other sensors were arranged accordingly. Thereafter, four signals were measured simultaneously, and the signals were received by the oscilloscope through four channels. The ECG and EMG signals were acquired through the Arduino module (AD8232, AD8226) acting as an interface, while the BP and MMG signals were directly extracted from the stacked sensor. All the signals were monitored using the oscilloscope.

Correlation between Cardiac- and Muscle-Related Biophysical Signals: The PTT refers to the time between the R peak in an ECG wave and the reference point of a pulse wave measured at the periphery of the body; in other words, it indicates the duration over which a pulsating pressure wave is delivered from the aortic valve to the peripheral part. The R peak of the ECG and the P1 peak of the BP were considered as indices representing the depolarization of the ventricle, and the time difference between the R and P1 peaks was calculated to determine the PTT. Here, the PTT was denoted as Δt_{be}. EMG and MMG signals are generated when muscle contractions are correlated with the ECG signals. This is because muscle movement alters the diameter and flow of blood vessels, which, in turn, affects cardiac activity. The time difference between the R peak of the ECG and the first exposure of the MMG signal was defined as Δ. MMG signals were selected because these are not electrically disturbed by the human body and its surroundings, unlike EMG signals. Furthermore, EMG signals were used for mutual verification with the MMG signals.

Supporting Information

Supporting Information is available from the Wiley Online Library or from the author.

Acknowledgements

This work was supported by Korea University Grants and the National Research Foundation of Korea (NRF) grant funded by the Korea government (MSIT) (NRF-2019R1A2C1002355 and NRF-2021R1A2B5B03001811). The authors acknowledge the assistance from the members of Multiscale Nature-Inspired Mechanics Laboratory (MNML). The authors would also like to thank Sharon Seohyun Chun

for drawing the parts of the human body. No ethical approval was needed for the experiments in this work, and the volunteer took part with informed consent.

Conflict of Interest

The authors declare no conflict of interest.

Data Availability Statement

The data that support the findings of this study are available from the corresponding author upon reasonable request.

Keywords

biophysical signals, cardiac health, cutaneous sensors, gels, multimodal strategies, sensors, wearable devices

Received: December 10, 2021
Revised: February 14, 2022
Published online: March 13, 2022

[1] a) K. O. Johnson, *Curr. Opin. Neurobiol.* **2001**, *11*, 455; b) A. Handler, D. D. Ginty, *Nat. Rev. Neurosci.* **2021**, *22*, 521; c) V. B. Mountcastle, R. H. LaMotte, G. Carli, *J. Neurophysiol.* **1972**, *35*, 122; d) D. W. Tan, M. A. Schiefer, M. W. Keith, J. R. Anderson, J. Tyler, D. J. Tyler, *Sci. Transl. Med.* **2014**, *6*, 1; e) F. Konietzny, H. Hensel, *Eur. J. Physiol.* **1977**, *368*, 39; f) W. R. Loewenstein, *J. Physiol.* **1956**, *133*, 588.

[2] a) J. Park, M. Kim, Y. Lee, H. S. Lee, H. Ko, *Sci. Adv.* **2015**, *1*, 1500661; b) M. Ha, S. Lim, J. Park, D.-S. Um, Y. Lee, H. Ko, *Adv. Funct. Mater.* **2015**, *25*, 2841; c) D.-I. Kim, T. Q. Trung, B.-U. Hwang, J.-S. Kim, S. Jeon, J. Bae, J.-J. Park, N.-E. Lee, *Sci. Rep.* **2015**, *5*, 12705; d) M. L. Jin, S. Park, Y. Lee, J. H. Lee, J. Chung, J. S. Kim, J.-S. Kim, S. Y. Kim, E. Jee, D. W. Kim, J. W. Chung, S. G. Lee, D. Choi, H.-T. Jung, D. H. Kim, *Adv. Mater.* **2017**, *29*, 1605973; e) K.-Y. Chun, Y. J. Son, S. Seo, H. J. Lee, C.-S. Han, *ACS Sens.* **2020**, *5*, 845; f) K.-Y. Chun, Y. J. Son, E.-S. Jeon, S. Lee, C.-S. Han, *Adv. Mater.* **2018**, *30*, 1706299.

[3] T. Yamada, Y. Hayamizu, Y. Yamamoto, Y. Yomogida, A. Izadi-Najafabadi, D. N. Futaba, K. Hata, *Nat. Nanotechnol.* **2011**, *6*, 296.

[4] a) Y. Khan, A. E. Ostfeld, C. M. Lochner, A. Pierre, A. C. Arias, *Adv. Mater.* **2016**, *28*, 4373; b) C. Wang, C. Wang, Z. Huang, S. Xu, *Adv. Mater.* **2018**, *30*, 1801368; c) S. P. Lee, G. Ha, D. E. Wright, Y. Ma, E. Sen-Gupta, N. R. Haubrich, P. C. Branche, W. Li, G. L. Huppert, M. Johnson, H. B. Mutlu, K. Li, N. Sheth, J. A. Wright Jr, Y. Huang, M. Mansour, J. A. Rogers, R. Ghaffari, *npj Digit Med.* **2018**, *1*, 2; d) Y.-D. Lee, W.-Y. Chung, *Sens. Actuators, B* **2009**, *140*, 390; e) M. K. Yapici, T. Alkhidir, Y. A. Samad, K. Liao, *Sens. Actuators, B* **2015**, *221*, 1469; f) N. Luo, W. Dai, C. Li, Z. Zhou, L. Lu, C. C. Y. Poon, S.-C. Chen, Y. Zhang, N. Zhao, *Adv. Funct. Mater.* **2016**, *26*, 1178; g) C. Dagdeviren, Y. Su, P. Joe, R. Yona, Y. Liu, Y.-S. Kim, Y. Huang, A. R. Damadoran, J. Xia, L. W. Martin, Y. Huang, J. A. Rogers, *Nat. Commun.* **2014**, *5*, 4496; h) C. Wang, X. Li, H. Hu, L. Zhang, Z. Huang, M. Lin, Z. Zhang, Z. Yin, B. Huang, H. Gong, S. Bhaskaran, Y. Gu, M. Makihata, Y. Guo, Y. Lei, Y. Chen, C. Wang, Y. Li, T. Zhang, Z. Chen, A. P. Pisano, L. Zhang, Q. Zhou, S. Xu, *Nat. Biomed. Eng.* **2018**, *2*, 687.

[5] a) S. Imani, A. J. Bandodkar, A. M. V. Mohan, R. Kumar, S. Yu, J. Wang, P. P. Mercier, *Nat. Commun.* **2016**, *7*, 11650; b) G. Bruno, S. Anastasova, G. Z. Yang, *Sensors* **2019**, *19*, 1616; c) Y. J. Hong, H. Lee, J. Kim, M. Lee, H. J. Choi, T. Hyeon, D.-H. Kim, *Adv. Funct. Mater.* **2018**, *28*, 1805754; d) Y. J. Son, J. W. Bae, H. J. Lee, S. Bae, S. Baik, K. -Y. Chun, C. -S. Han, *J. Mater. Chem. A* **2020**, *8*, 6013.

[6] a) Y. Yoon, J. H. Cho, G. Yoon, *J. Med. Syst.* **2009**, *33*, 266; b) R. C. Block, M. Yavarimanesh, K. Natarajan, A. Carek, A. Mousavi, A. Chandrasekhar, C. S. Kim, J. Zhu, G. Schiftto, L. K. Mestha, O. T. Inan, J. O. Hahn, R. Mukkamala, *Sci. Rep.* **2020**, *10*, 16373; c) R. A. Payne, C. N. Symeonides, D. J. Webb, S. R. J. Maxwell, *J. Appl. Physiol.* **2006**, *100*, 136.

[7] T. Wibmer, S. Rüdiger, D. Scharnbeck, M. Radermacher, S. Markovic, K. M. Stoiber, W. Rottbauer, C. Schumann, *Echocardiography* **2015**, *32*, 904.

[8] S. Chun, J.-S. Kim, Y. Yoo, Y. Choi, S. J. Jung, D. Jang, G. Lee, K.-I. Song, K. S. Nam, I. Youn, D. Son, C. Pang, Y. Jeong, H. Jung, Y.-J. Kim, B.-D. Choi, J. Kim, S.-P. Kim, W. Park, S. Park, *Nat. Electron.* **2021**, *4*, 429.

[9] a) Y. Kim, A. Chortos, W. Xu, Y. Liu, J. Y. Oh, D. Son, J. Kang, A. M. Foudeh, C. Zhu, Y. Lee, S. Niu, J. Liu, R. Pfattner, Z. Bao, T.-W. Lee, *Science* **2018**, *360*, 998; b) Y. R. Lee, T. Q. Trung, B.-U. Hwang, N.-E. Lee, *Nat. Commun.* **2020**, *11*, 2753.

[10] T. Hwang, Z. Frank, J. Neubauer, K. J. Kim, *Sci. Rep.* **2019**, *9*, 9658.

[11] Y. Zhang, J. Liu, Y. Zhang, J. Liu, Y. Duan, *RSC Adv.* **2017**, *7*, 54031.

[12] a) L. A. Geddes, M. E. Valentinuzzi, *Ann. Biomed. Eng.* **1973**, *1*, 356; b) A. Searle, L. Kirkup, *Physiol. Meas.* **2000**, *21*, 271.

[13] a) J. Rivnay, S. Inal, A. Salleo, R. M. Owens, M. Berggren, G. G. Malliaras, *Nat. Rev. Mater.* **2018**, *3*, 1; b) D. Mawad, A. Artzy-Schnirman, J. Tonkin, J. Ramos, S. Inal, M. M. Mahat, N. Darwish, L. Zwi-Dantsis, G. G. Malliaras, J. J. Gooding, A. Lauto, M. M. Stevens, *Chem. Mater.* **2016**, *28*, 6080; c) S. Xia, S. Song, F. Jia, G. Gao, *J. Mater. Chem. B* **2019**, *7*, 4638; d) J. Yang, C. R. Han, J. F. Duan, F. Xu, R. C. Sun, *Nanoscale* **2013**, *5*, 10858; e) C. Hu, J. Zhang, X. Wang, L. Xing, L. Shi, R. Ran, *ACS Appl. Mater. Interfaces* **2018**, *10*, 44000.

[14] a) X. Xiao, G. Wu, H. Zhou, K. Qian, J. Hu, *Polymers* **2017**, *9*, 259; b) T. Shay, O. D. Velev, M. D. Dickey, *Soft Matter* **2018**, *14*, 3296; c) P. A. Lopes, D. V. Gomes, D. G. Marques, P. Faia, J. Góis, T. F. Patrício, J. Coelho, A. Serra, A. T. de Almeida, C. Majidi, M. Tavakoli, *Adv. Healthcare Mater.* **2019**, 1900234; d) S. Mandal, A. Seth, V. Yadav, S. Kumari, M. Kumar, U. Ojha, *ACS Appl. Polym. Mater.* **2020**, *2*, 618; e) H. Wu, G. Yang, K. Zhu, S. Liu, W. Guo, Z. Jiang, Z. Li, *Adv. Sci.* **2021**, *8*, 2001938.

[15] a) K. Niizeki, Y. Miyamoto, *Am. J. Physiol.* **1999**, *276*, H1331; b) G. Giuriato, S. J. Ives, C. Tarperi, L. Bortolan, F. Ruzzante, A. Pedrinolla, C. Martignon, F. G. Laginestra, A. Cevese, F. Schena, M. Venturelli, *J. Appl. Physiol.* **2020**, *128*, 805.

[16] a) R. L. Kirby, D. A. MacLeod, A. E. Marble, *Angiology* **1989**, *40*, 620; b) R. L. Kirby, S. T. Nugent, R. W. Marlow, D. A. MacLeod, A. E. Marble, *J. Appl. Physiol.* **1989**, *66*, 323.

[17] T. Kimura, N. Kameda, T. Moritani, *J .Electromyogr. Kinesiol.* **2010**, *20*, 572.

[18] T. W. Beck, T. J. Housh, J. T. Cramer, J. P. Weir, G. O. Johnson, J. W. Coburn, M. H. Malek, M. Mielke, *Biomed. Eng.* **2005**, *4*, 1.

[19] a) Y. Yoshitaka, M. Shinohara, H. Ue, T. Moritani, *J. Appl. Physiol.* **2002**, *93*, 1744; b) S. Noh, C. Yoon, E. Hyun, H. N. Yoon, T. J. Chung, K. S. Park, H. C. Kim, *Electron. Lett.* **2014**, *50*, 143.